





# Double-layer technique for welding subsea joints without post welding heat treatment

George Luiz Gomes de Oliveira<sup>1</sup> , Hélio Cordeiro de Miranda<sup>2</sup> , Edvan Cordeiro de Miranda<sup>1</sup> , Pedro Helton Magalhães Pinheiro<sup>1</sup> 

<sup>1</sup> Universidade Federal do Ceará – UFC, Campus Russas, Russas, CE, Brasil.

<sup>2</sup> Universidade Federal do Ceará – UFC, Departamento de Engenharia Metalúrgica e de Materiais, Campus do Pici, Fortaleza, CE, Brasil.

**How to cite:** Oliveira GLG, Miranda HC, Miranda EC, Pinheiro PHM. Double-layer technique for welding subsea joints without post welding heat treatment. *Soldagem & Inspeção*. 2022;27:e2707. <https://doi.org/10.1590/0104-9224/SI27.07>

**Abstract:** Welded joints for subsea systems are usually buttered with a nickel alloy, heat-treated and then joined together. Although the majority of these joints have been successful throughout their service, some have suffered catastrophic failure, leading to investigations into the possible causes. The use of heat treatment has been considered the primary cause for failure in this type of joint. The main objective of this article is, with background on the methodology used on Double-Layer Controlled Deposition Technique – DL-CDT, along with the LPTS decision diagrams, to determine the relations between the buttering parameters that allow the welding of subaquatic joints, and the low need for heat treatment. MIG single-bead-on-plate welding was executed on samples of AISI 8630M steel. The welded samples were submitted to metallographic analyses of their geometric and microstructural characteristics and the confection of decision diagrams. Among the 200 possible relationships between the buttering parameters, only one presented positive gaps over all criteria. Grain refinements were observed in the HAZ of joints buttered for the parameters approved by the decision diagrams, while for the joints submitted to the Post Welding Heat Treatment (PWHT) peaks of microhardness on the buttering interface were found, which may result in fragilization of that region.

**Key-words:** Subsea joints; PWHT; Double layer technique; LPTS criterion.

## 1. Introduction

Welded joints are commonly used in subsea systems for oil and gas production. Such connections are usually buttered with a nickel alloy (generating a dissimilar interface), heat treated (Post Welding Heat Treatment – PWHT) and then joined, without the necessity for post-weld heat treatment on this final joint. Although the majority of these joints have satisfactory results, some have suffered catastrophic failure, which has led to investigations into the possible causes [1-3].

PWHT also aims to control the resulting hardness along the Heat Affected Zone – HAZ formed when connecting high resistance steels and to create a maximum hardness level of 22 HRC (250 HV) as established by the NACE MR0175 norm [4], minimizing the possibility of joint fragilization due to the presence of hydrogen.

However, PWHT in the post buttering process has been considered [5,6] an agent responsible for some undesirable phenomena, such as carbide precipitation and, consequently hardening and fragilization of the dissimilar buttered interface region. OLDEN et al. [7] made a series of measurements of the hydrogen levels of subsea joints, in the as welded condition, and in subsea joints, submitted to PWHT. These authors suggested that the intense carbide precipitation may, beside fragilizing the dissimilar interface, lead to the capture of H<sup>+</sup> ions diffused along the joint, which increases the possibility of failure due to hydrogen fragilization.

The use of welding procedures that allow buttering without the need for PWHT, could well be a solution to overcome the possible precipitation and fragilization of the interface as mentioned. The Double-Layer Controlled Deposition Technique (DL-CDT) aims to promote an adequate superposition of the heat cycles, so that the deposited second layer will promote the refinement and tempering of the HAZ with higher grain sizing from the first layer, as well as reduce the sensitivity to joint fissures. The DL-CDT technique considers the hardness and microstructure criteria proposed by Higuchi [8-12].

However, the DL-CDT is extremely sensitive to changes in welding parameters, requiring strict control during the welding procedure. The Laboratório de Pesquisa e Tecnologia de Soldagem - (LPTS) has developed, over the past few years, a variety of research works applying the DL-CDT, using different materials and welding procedures [8,13-15].

In addition, LPTS developed a method to visualize the results as well as to define the limits of hardness and microstructure as proposed by Higuchi, more clearly. This method allows the possibility to modify Higuchi equations and present them, for a set of parameters, in a single graph, called a decision diagram. The application of the parameter choice methodology of the DL-CDT, along with decision diagrams for the analysis of welding procedures has the potential not only to reduce manufacturing costs associated to the PWHT stage, but also to minimize fragilization of the dissimilar steel-nickel interface [8,12-14].

Received: 11 Mar., 2022. Accepted: 12 Apr., 2022.

E-mails: georgeluz@ufc.br (GLGO), hmiranda@ufc.br (HCM), edvan@ufc.br (ECM), pedrohelton@ufc.br (PHMP)



This is an Open Access article distributed under the terms of the [Creative Commons Attribution Non-Commercial License](https://creativecommons.org/licenses/by-nc/4.0/) which permits unrestricted non-commercial use, distribution, and reproduction in any medium provided the original work is properly cited.

In this context, the aim of this work is to apply both the hardness and microstructure criteria in DL-CDT, as well as the decision diagrams proposed by LPTS, to determine the parameters for buttering and their relationships that allow manufacturing of joints with a low need for PWHT.

## 2. Materials and Methods

### 2.1. Materials

AISI 8630M and ASTM A182 F22 steels were used as the base metals and the AWS ERNiCrMo-3 and AWS ER80S-D2 electrodes, with a 1.2 mm diameter, were used as the filler metals. Table 1 and Table 2 present the chemical compositions of these materials.

**Table 1.** Composition values in wt% for the base metals (obtained by optic emission spectroscopy).

Base metal	Composition values, wt %								
	C	Si	Mn	Cr	Ni	Mo	P	Cu	Al
AISI 8630M	0.36	0.30	0.86	0.93	0.81	0.38	0.006	0.06	0.02
ASTM A182 F22	0.12	0.17	0.40	2.25	0.06	0.93	0.012	0.04	0.024

**Table 2.** Composition values in wt% for the filler metals (provided by the manufacturer).

Electrode AWS	Composition values, wt %								
	C	Si	Mn	Mo	Ni	Cr	Fe	Al	Nb
ERNiCrMo-3	0.011	0.05	0.01	9.13	64.43	22.2	0.19	0.09	3.53
ER80S-D2	0.10	0.70	1.70	0.50	-	-	97.00	-	-

### 2.2. Experimental procedure

Robotized MIG welding was executed from a flat position, with a single pass, on AISI 8630M steel samples with dimensions of 150 x 50 x 30 mm in the hardened and tempered condition (maximum hardness 250 HV, in accordance to the NACE MR0175 norm [4]). The pre-heat temperature was maintained at 300 °C. The shielding gas used was a gas mixture of 75% argon and 25% helium.

An experiment table was prepared showing the variation of heat input (in three levels), the energy technique, the weaving arc movement applied and the electrode used, being the last three presented in two levels. Table 3 shows the weld parameters used.

**Table 3.** MIG Bead-on-plate welding parameters.

Sample name	$I_{RMS}$ (A)	Heat input (kJ/mm)	Volts (V)	Travel speed (m/min)	Energy technique	Arc Weaving	Electrode AWS
N6INW	147	0.6	25	0.4	I	NW	ERNiCrMo-3
N9RNW	195	0.9	29	0.4	R	NW	ERNiCrMo-3
N12INW	250	1.2	33	0.4	I	NW	ERNiCrMo-3
N6TNW	195	0.6	29	0.5	T	NW	ERNiCrMo-3
N12TNW	195	1.2	29	0.3	T	NW	ERNiCrMo-3
N6ITW	147	0.6	25	0.4	I	TW	ERNiCrMo-3
N9RTW	195	0.9	29	0.4	R	TW	ERNiCrMo-3
N12ITW	250	1.2	27	0.4	I	TW	ERNiCrMo-3
N6TTW	195	0.6	29	0.5	T	TW	ERNiCrMo-3
N12TTW	195	1.2	29	0.3	T	TW	ERNiCrMo-3
C6INW	152	0.6	25	0.4	I	NW	ER80S-D2
C9RNW	195	0.9	29	0.4	R	NW	ER80S-D2
C12INW	250	1.2	33	0.4	I	NW	ER80S-D2
C6TNW	195	0.6	29	0.5	T	NW	ER80S-D2
C12TNW	195	1.2	29	0.3	T	NW	ER80S-D2
C6ITW	152	0.6	25	0.4	I	TW	ER80S-D2
C9RTW	195	0.9	29	0.4	R	TW	ER80S-D2
C12ITW	250	1.2	33	0.4	I	TW	ER80S-D2
C6TTW	195	0.6	29	0.5	T	TW	ER80S-D2
C12TTW	195	1.2	29	0.3	T	TW	ER80S-D2

I – heat input obtained by change in current. T – heat input obtained by change in travel speed. R – reference. NW – no arc weaving. TW – triangular arc weaving.

After which, the regions next to the beginning and end of the weld bead (20 mm from each) were cut off from the specimens, which then underwent metallographic preparation for microhardness profile analyses along the HAZ formed, in order to determine the soft and hard zones. Vickers microhardness tests were performed at maximum penetration region of the weld bead, with a load of 100 g and the distance between the impressions was 0.2 mm. In addition measurements of the geometric (reinforcement and penetration, mainly) and microstructural (extensions of the Heat Affected Zone with Coarse Grains – HAZCG and the Heat Affected Zone with Fine Grains – HAZFG) characteristics were performed to make the decision diagrams with basis on the hardness and the microstructure criteria [8, 9].

### 2.2.1. Construction of the decision diagrams

Once the values of the extension of the hard and soft zones and the geometric characteristics of the generated beads had been found, decision diagrams were assembled based on the methodology proposed by LPTS [8], for two possible conditions of buttering: using the ERNiCrMo-3 electrode and the ER80S-D2 electrode. Four equations were used for the two acceptance criteria (tempering and refinement) to make the two decision diagrams.

- Hardness criterion (tempering) (Equations 1 and 2)

$$1) DSZ_2 - DHZ_1 > 0 \quad (1)$$

Where:  $DSZ_2$  = depth of the second layer soft zone;  
 $DHZ_1$  = depth of the first layer hard zone.

$$2) (R_1 + P_1) - DHZ_2 > 0 \quad (2)$$

Where:  $DHZ_2$  = depth of the second layer hard zone;  
 $R_1$  = Reinforcement of the first layer;  
 $P_1$  = Penetration of the first layer.

- Microstructure criterion (refinement) (Equations 3 and 4)

$$1) DHAZFG_2 - DHAZCG_1 > 0 \quad (3)$$

Where:  $DHAZFG_2$  = depth of the second layer HAZFG;  
 $DHAZCG_1$  = depth of the first layer HAZCG.

$$2) MZ_1 - DHAZCG_2 > 0 \quad (4)$$

Where:  $DHAZCG_2$  = depth of the second layer HAZCG;  
 $MZ_1$  = melted zone of the first layer.

### 2.2.2. Joint welding for subsea applications

After production of the decision diagrams, some combinations of parameters were chosen, and specimens were manufactured by simulating the weld of AISI 8630M steel joints for subsea applications. However, for the buttered specimens with combinations of parameters approved by both hardness and microstructure criteria, the PWHT was not applied. Exclusively, one specimen (S2) was buttered using the parameters approved by the hardness and microstructure criteria and submitted to PWHT so that the influence of the latter could be evaluated separately. The relationships between the chosen parameters for the buttering stage of the manufactured specimens can be seen in Table 4.

**Table 4.** Relationships between the chosen parameters for the buttering of the manufactured specimens.

Sample	First Layer	Further Layers	Base Material	PWHT
S1	N6TNW	N12TTW	8630M	No
S2	N6TNW	N12TTW	8630M	Yes
S3	N6TNW	N6TNW	8630M	No
S4	N6INW	N6INW	8630M	Yes
S5	N6TNW	N12TTW	F22	No
S6	N6INW	N6INW	F22	Yes

Although the decision diagrams criteria were not applied to the ASTM A182 F22 steel (chemical composition on Table 1), the resulting welding parameters of the studies done on the AISI 8630 steel were used for the confection of welded joints using

that material. The choice of the same parameters used on the AISI 8630M is justified by the similarity of the equivalent carbon for those steels (0.8 according to the *International Institute of Welding – IIW* equation, for both) and the more critical hardness condition, as there is a higher carbon content in the AISI 8630M steel.

### 3. Results and Discussion

#### 3.1. Construction of the decision diagrams

The geometry and superficial aspect of two weld beads obtained with AISI 8630M steel according to the parameters presented in Table 3 are shown in Figure 1.

A weld with a “goblet” shaped penetration profile can be seen for the welds that were performed without arc weaving and a more homogeneous profile with the ones with triangular arc weaving.

The majority of the resulting geometry and superficial aspects of the welds were regular and of good quality. Such a result was already expected since in all conditions a spray droplet transfer mode was sought and a stable welding arc was observed, using a pulsating current.

However, even though the shielding gas used was composed of 25% helium, most of the welds presented a “goblet” shaped penetration profile. This effect was intensified on the welds performed with the ERNiCrMo-3 electrode and probably occurred because of the characteristics of the filler metal in that group of welds. The use of arc weaving reduced that effect for both electrodes.

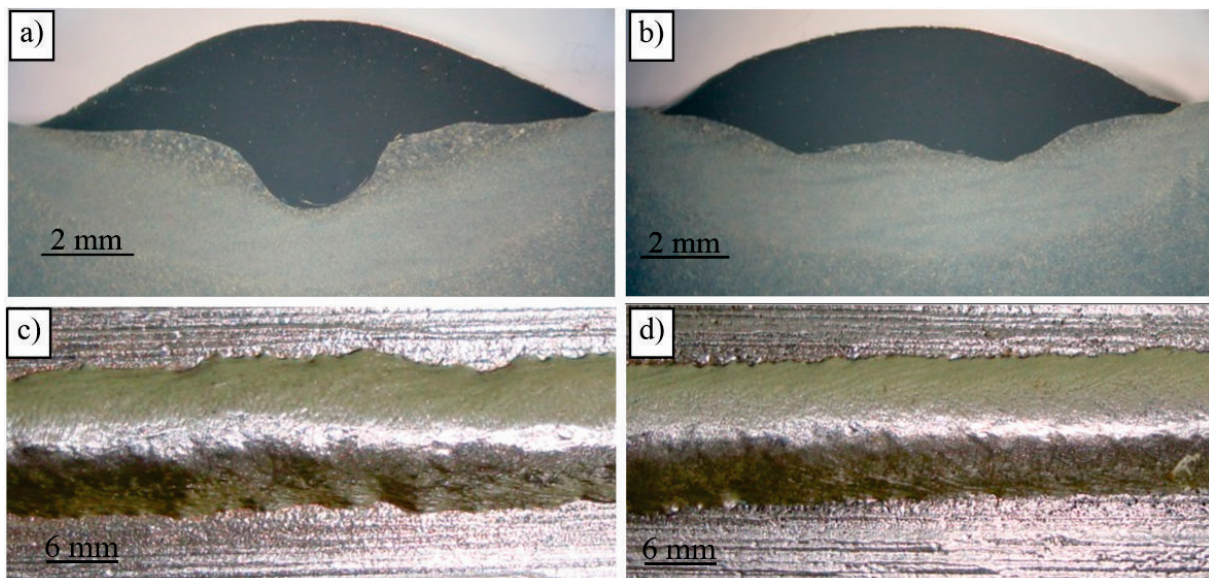


**Figure 1.** Cross section of the welds performed with the ERNiCrMo electrode. a) and c) 0.6 kJ/mm, type T, no arc weaving. b) and d) 0.6 kJ/mm, type T, with triangular arc weaving.

Another important characteristic observed in most of the samples that were welded with AISI 8630M, was the presence of possible base metal previous banding, which characterize heterogeneities in the chemical composition, in the HAZ of the welds. Figure 2 shows a macrograph of a sample with banding (white arrows) in the HAZ.

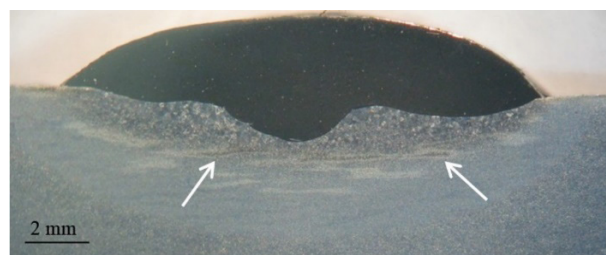


**Figure 2.** Welded Sample with banding in the HAZ.

The phenomenon of banding is well known among steels, especially for medium and high carbon content steels [10,16-21]. Banding is usually associated to two primary causes:

The first cause is associated to carbon (C) which, by possessing a higher diffusion coefficient than most of the other alloy elements, tends to segregate, either during the solidification (presegregation), or during the transformations into the solid state (transsegregation) [19].

The second cause is related to elements that reduce the initial temperature for ferrite formation, like manganese (Mn), nickel (Ni) and chrome (Cr). This delay to the beginning of ferrite formation leads to a greater C content in the resulting austenite [10].

A large majority of the studies cited here confirm that the banding phenomenon is hard to eliminate. Even after applying annealing heat treatments for prolonged intervals, which enables the diffusion of the segregated elements, a complete homogenization of the chemical and mechanical properties of the banded steels is not achieved.

The bands found in the welded samples in this stage lead to the formation of hardness gradients throughout the HAZ and made it harder to use the hardness criteria.

Figure 3 shows a typical microhardness profile found in the analyzed welds. This profile was taken as the basis for measuring the extension of the hard zone – HZ and the soft zone – SZ. The value of 325 HV was considered to be the inferior limit for the HZ and consequently the superior limit for the SZ, and 250 HV was the inferior limit for the SZ. The limits of the HZ and the SZ were determined according to the NACE MR0175 norm [4]. The inferior limit of 250 HV for SZ is a value that is the maximum hardness for base metals used in subsea joints. The value of 325 HV was used for the inferior limit of the HZ, which is the maximum hardness for the HAZs of these joints, in the case of sulfur free environments.

However, even with the use of an elevated preheat temperature of 300°C, the increase of hardness in the material, as a consequence of the welding thermal cycle, was considerable and reached levels in the order of 600 HV.

The elevated values of microhardness found in the HAZs of the analyzed welds were expected because of the high carbon content present in the AISI 8630M steel (0.36%) and its elevated carbon equivalent (0.8, according to the IIW equation).

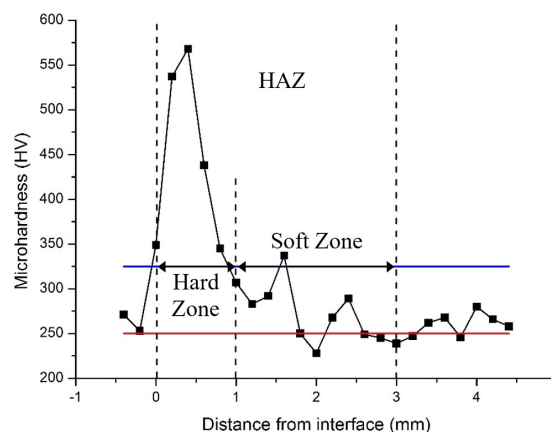


**Figure 3.** Microhardness profile for the AISI 8630M steel welded with the ERNiCrMo-3 electrode with heat input set to 0.6 kJ/mm and no arc weaving.

The values of the extension of the HZ and SZ can be seen in Table 5 for the regions at the beginning and end of the beads generated with nickel (ERNiCrMo-3) and low carbon (ER80S-D2) electrodes, measured using the microhardness graphs developed.

**Table 5.** Values for HZ extension and SZ extension measured in MIG bead-on-plate welding (Table 3).

Specimen	Nickel - Beginning		Nickel - End		Carbon - Beginning		Carbon - End	
	HZ (mm)	SZ (mm)	HZ (mm)	SZ (mm)	HZ (mm)	SZ (mm)	HZ (mm)	SZ (mm)
(N or C)6INW	1.7	0.5	1.9	0.9	2.2	1.4	2.1	1.3
(N or C)6ITW	2.2	0.8	2.0	1.4	2.2	0.8	1.9	1.1
(N or C)6TNW	1.3	0.9	0.9	1.9	1.7	0.5	1.8	0.8
(N or C)6TTW	1.9	1.1	1.3	1.1	2.0	0.8	2.2	0.8
(N or C)9RNW	2.0	1.0	2.0	0.8	2.0	1.4	1.7	1.3
(N or C)9RTW	1.8	1.0	2.0	1.0	2.0	1.4	2.1	0.9
(N or C)12INW	2.0	1.2	1.4	1.0	1.9	0.9	1.9	1.3
(N or C)12ITW	2.1	1.1	1.9	1.7	1.6	1.6	1.7	1.7
(N or C)12TNW	2.2	1.4	2.4	1.2	1.6	1.8	2.0	1.8
(N or C)12TTW	2.3	1.9	1.8	2.0	1.8	1.8	2.3	1.1

Table 5 shows that higher extensions of HZs and SZs are related to samples welded with higher heat input and triangular arc weaving. Analyses related to the extension of the HZs and SZs are more difficult to perform because of the banding found in the AISI 8630M steel as well as due to the single pass welding executed using the material in the application conditions, hardened, and tempered and not only hardened [9], which further complicates the possibility of making precise measurements for the SZ.

The difficulty of the analyses is represented in Figure 4, where only tendencies of the effects of the heat input and of the arc weaving can be seen, with no statistical meaning for some of the results.

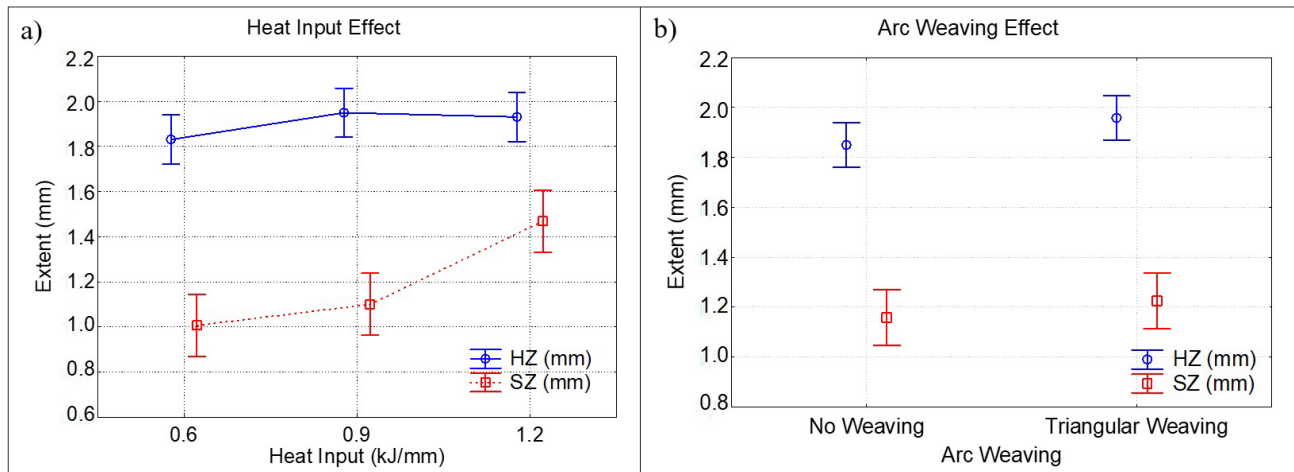


Figure 4. Statistical analysis of the effects of a) heat input, and b) type of weaving, over the extensions of the hard and soft zones.

Table 6 shows the values of reinforcement (R) and penetration (P) measured for welding parameters shown in Table 3. These values, along with the hard and soft zones are necessary for the construction of the decision diagrams.

Table 6. Values of reinforcement (R) and penetration (P) measured in MIG bead-on-plate welding (Table 3).

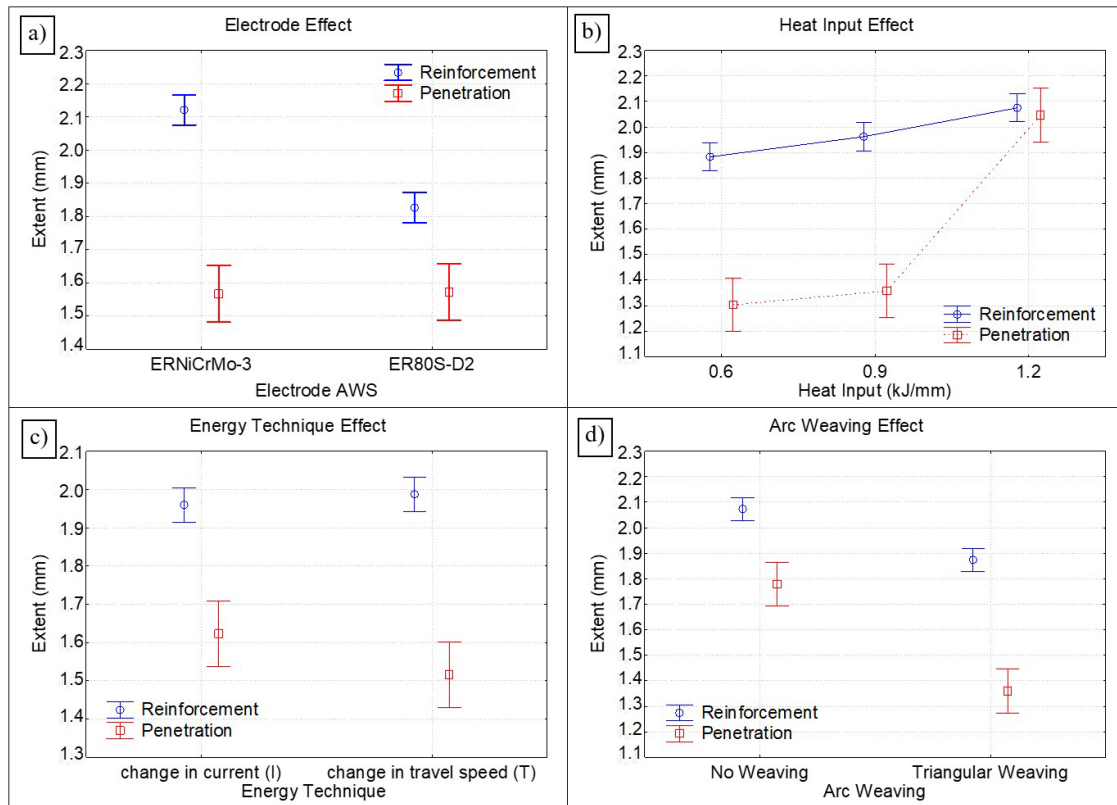
Specimen	Nickel - Beginning		Nickel - End		Carbon - Beginning		Carbon - End	
	R (mm)	P (mm)	R (mm)	P (mm)	R (mm)	P (mm)	R (mm)	P (mm)
(N or C)6INW	2.3	1.3	2.2	1.1	1.7	1.3	1.8	1.2
(N or C)6ITW	2.1	0.9	2.1	0.8	1.6	1.2	1.5	1.3
(N or C)6TNW	1.9	1.9	2.0	2.0	1.9	1.4	1.9	1.4
(N or C)6TTW	1.9	1.2	1.8	1.3	1.7	1.4	1.9	1.3
(N or C)9RNW	2.3	1.4	2.1	1.7	1.8	1.4	1.8	1.6
(N or C)9RTW	2.0	1.2	1.8	1.2	2.0	1.3	1.9	1.0
(N or C)12INW	2.5	2.2	2.5	3.1	1.9	2.9	1.6	2.5
(N or C)12ITW	2.3	2.0	2.3	2.1	1.7	2.2	1.5	2.2
(N or C)12TNW	2.5	2.1	2.4	1.7	2.4	2.3	2.4	2.2
(N or C)12TTW	1.7	1.2	2.1	1.8	1.9	1.3	1.7	1.2

Figure 5 shows that the results found for the geometry of the weld bead (shown in Table 6), differently from the ones found for the soft and hard zones, were statistically significant.

The ERNiCrMo-3 electrode presented greater reinforcement than the ER80S-D2 electrode. This effect was associated primarily to the lower wettability inherent to welding with a nickel alloy. Another characteristic of that group of welds was the use of a higher feed rate, compared to the ones executed with the ER80S-D2 electrode. In order that a systematic analysis of the control parameters could be carried out, the effective current was kept constant whenever another parameter was under study.

Also due to the higher number of alloy elements in the ERNiCrMo-3 electrode and, consequently, a higher resistivity and fusion rate, the feed rate for that group of welds was increased, so that the arc length and other parameters could be kept constant. This increase in feed rate also contributed to a greater reinforcement found in the welds using the ERNiCrMo-3 electrode.





**Figure 5.** Statistical analyses of the effects of a) the electrode, b) heat input, c) the energy technique and d) of the type of arc weaving over the reinforcement and the penetration.

Another statistically significant effect was arc weaving over the reinforcement and penetration. Figure 5d shows that with the use of triangular weaving (TW) their values went down. This was due to a better distribution of the deposited material in relation to the no weaving condition. Similar results have been reported in other papers [22,23].

Figure 6 presents one of the decision diagrams (elaborated according to [8]) used in the definition of the best parameter relationships for buttering pointed by the hardness and microstructure criteria.

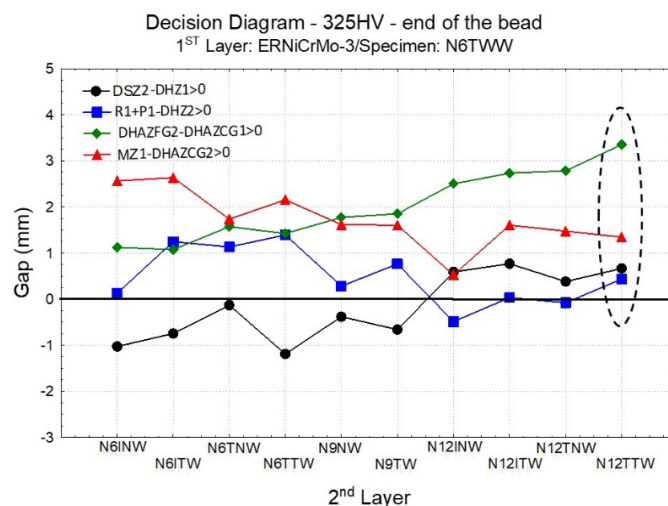


**Figure 6.** Example of decision diagram for a condition met by both hardness and microstructure criteria.

These decision diagrams were constructed in two great clusters: the diagrams elaborated with buttering using the ERNiCrMo-3 electrode and the diagrams elaborated with buttering using the ER80S-D2 electrode.

Among the 200 possibilities of parameter relationships for buttering, only one presented positive gaps in all aspects, considering the fulfillment of the criteria simultaneously at the beginning and end of the bead. This is demonstrated in Table 7.

However, no parameter relationships that met the hardness and microstructure criteria could be found with buttering when using the ER80S-D2 electrode.

**Table 7.** Parameter relationships met by both hardness and microstructure criteria in the AISI 8630M steel.

1 <sup>ST</sup> Layer	2 <sup>ND</sup> Layer	DSZ <sub>2</sub> -DZH <sub>1</sub> [mm]		(R <sub>1</sub> +P <sub>1</sub> )-DZH <sub>2</sub> [mm]	
		Beginning	End	Beginning	End
N6TNW	N12TTW	0.3	0.7	0.3	0.4

The minimum quantity of approved relationships is primarily related to the hardness criterion, which is a function of the high hardenability, the carbon content and the low  $A_{c1}$  temperature of the AISI 8630M steel. Another critical factor for the hardness criterion for the AISI 8630M steel is the presence of strong banding, as mentioned previously, which hinders a more precise measurement of the hard and soft zones.

The decision diagrams demonstrated that the deposition of the first layer with low heat input, the primary criterion for tempering ( $DSZ_2 > DZH_1$ ), was not achieved when conditions of low heat input were also used for the second layer. In these cases, the isothermals responsible for tempering the HAZ of the first pass generated by the parameters of low heat input of the second layer would not affect the hard zones of the first layer completely.

However, as higher heat input parameters are applied to the second layer that latter mentioned problem is reduced and positive gap values begin to appear. On the other hand, the second criterion of tempering ( $R_1 + P_1 > DZH_2$ ), which for the low heat input on the second layer did not present an issue, begins to show negative gap values in function of the low reinforcement and penetration values, when compared to the extensions of the hard and soft zones.

When high heat input is applied for the deposition of the first layer, the first criterion of tempering ( $DSZ_2 > DZH_1$ ) provokes problems for all heat input levels of the second layer, and is associated primarily to the elevated depths of the hard zone generated by that situation. A progression in that aspect can be observed as the heat input for the second layer is increased, however, that progression was not enough to generate positive gaps.

The single pass welding does not contemplate some aspects of the stage of deposition in layers, with the increase in reinforcement of the first layer due to the superposition of passes and, for this paper, the change in a steel substrate for nickel substrate (in the case of deposition of the second layer).

These factors, along with the necessity of deposition of many layers for the execution of buttering, lead to the evaluation of the manufacturing of a joint welded with a condition (relation of parameters) with gaps close to being approved. The S3 sample, presented in Table 4, was buttered with a condition of that type.

Table 8 shows the gaps of the parameter relationship used for the S3 sample buttering. That parameter relationship presented issues only for the first criterion (hardness) and primarily only at the beginning of the bead (region of lower significance in the confection of real joints), and therefore it qualified for the evaluation in a welded joint.

**Table 8.** Parameter relationship used on buttering of sample S3.

1 <sup>ST</sup> Layer	2 <sup>ND</sup> Layer	DSZ <sub>2</sub> -DZH <sub>1</sub> [mm]		(R <sub>1</sub> +P <sub>1</sub> )-DZH <sub>2</sub> [mm]	
		Beginning	End	Beginning	End
N6TNW	N6TNW	-1.0	-0.1	0.6	1.1

The conditions studied in the single pass welding stage allowed parameter relationships to be chosen, indicated or not, by the decision diagrams and then the effectiveness of these methodologies could be evaluated in the manufacturing of joints for subsea applications. The results of this analysis are presented next.

### 3.2. Joints for subsea applications

Macrographs for some specimens are shown in Figure 7, which were used to simulate the welding of joints for subsea applications. As described in the experimental procedure, the buttered specimens with parameter relationships that were approved in the decision diagrams were not submitted (except for S2) to PWHT after buttering, while the other ones were manufactured according to the procedure described in the Introduction of this paper.

Microstructures commonly found in the HAZ of samples welded with AISI 8630M steel are shown in Figure 8. The microstructure found in samples welded with the conditions indicated by the decision diagrams can be found in Figure 8a, while the microstructure found in samples welded with the conditions that did not meet the hardness and microstructure criteria can be seen in Figure 8b.



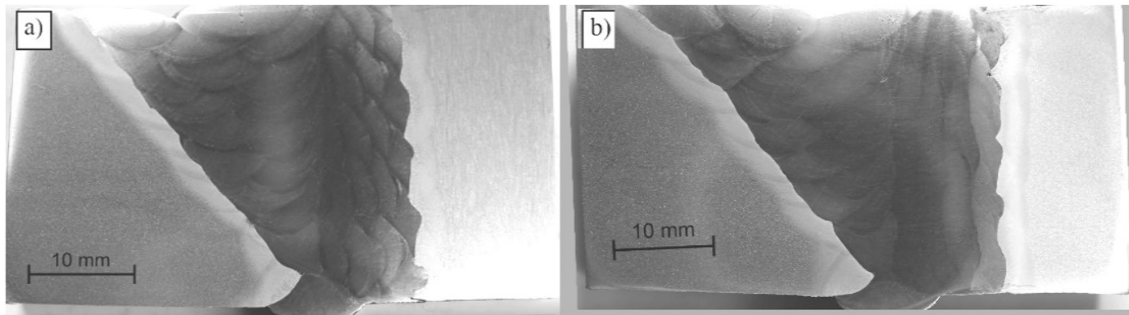


**Figure 7.** Examples of specimens macrographs manufactured to simulate the welding of joints for subsea applications. (a) S2. (b) S4.

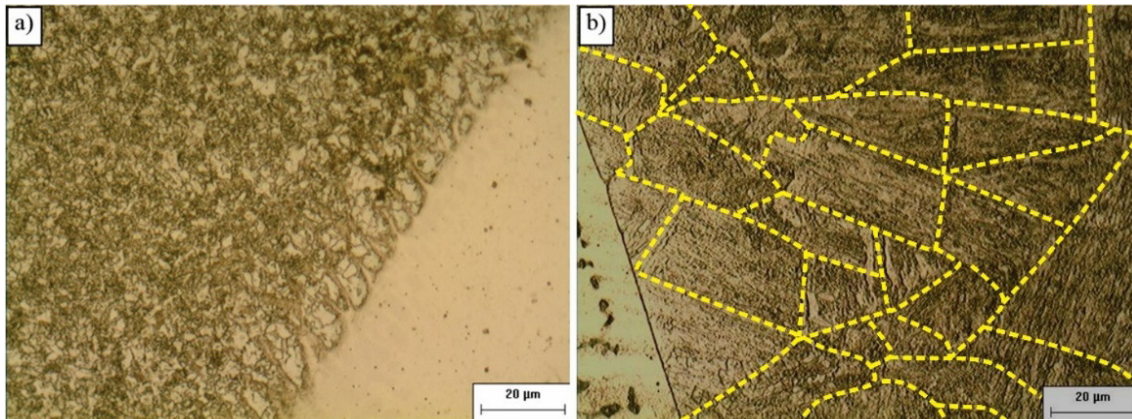


**Figure 8.** HAZ mostly found in samples welded with conditions a) approved and b) not approved by the hardness and microstructure criteria.

The microstructure found was basically composed of tempered martensite for both welding conditions used (approved or not approved by the selected criteria).

Figure 8a represents the general behavior seen in the HAZ of the buttered samples with conditions approved by the decision diagrams. An intense grain refinement of HAZ can be observed even in regions close to the dissimilar interface, where a coarse grains region is often found.

The substitution of a microstructure with coarse grains for a refined one, in ferritic steels with medium and low carbon, is indicated as an effective way to increase the toughness of the material. The higher the size of the grain, the greater the sliding bands and greater the stress concentration. With greater stress concentration, micro cracks are introduced to the grain boundaries, causing fracture by material cleavage.

In samples welded with conditions not meeting the selected criteria (Figure 8b) the presence of coarse grains in a significant portion of the HAZ are formed by the buttering, which, according to the data in the previous paragraph, can compromise the toughness of these regions even after tempering with PWHT.

The microstructural effect of refinement on the HAZ of the buttered specimens for parameters that met the selected criteria were also observed in the joints manufactured with ASTM A182 F22 steel, although for that steel, the microstructure found is basically composed of tempered martensite and bainite.

Figure 9 shows the hardness profiles in three regions (top, middle and root) of the cross section of two welded joints. The maximum, minimum and average hardness values found in the HAZ (up to 1mm from the dissimilar interface) of the respective joint are also indicated.

The hardness values found were similar for the three regions analyzed and only the samples submitted to PWHT met the maximum hardness criterion required by the NACE MR0175 norm [4].

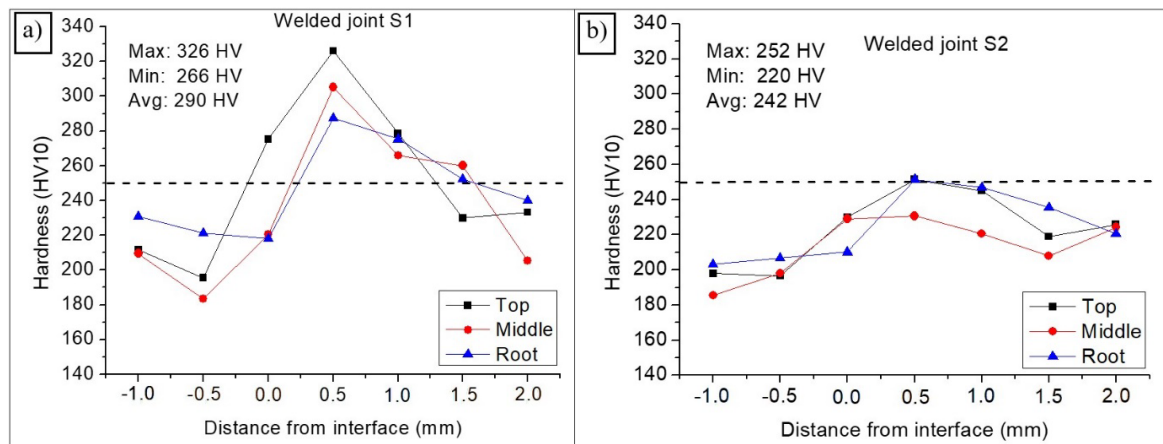


Figure 9. Hardness profiles for the joints welded with AISI 8630M steel and buttered with the parameter approved by the decision diagrams a) without PWHT and b) with PWHT.

Figure 10 presents an analysis of the variance of the effects of the steel and buttering technique used on the hardness found in the HAZ (up to 1mm from the dissimilar interface) of the studied joints.

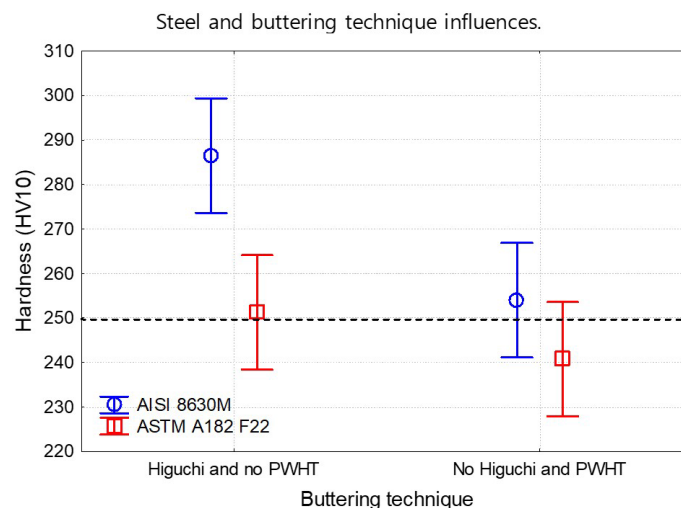


Figure 10. Analysis of variance of the steel and buttering technique used.

With the buttering procedure using parameters that met the selected criteria, the ASTM A182 F22 steel presented lower hardness levels than the AISI 8630M steel; however, this result was already expected due to the lower carbon content in the former. While for a conventional buttering procedure, or more specifically, the deposition of layers using parameters that did not meet the selected criteria, followed by PWHT, did not show any significant differences between the two steels.

A tendency of hardness reduction was seen in the joints buttered using the conventional buttering procedure (cited in the previous paragraph). This reduction was significant for the AISI 8630M steel, while for the ASTM A182 F22 steel it was not.

The greater hardness levels presented by the joint buttered with the parameters proposed by the decision diagrams without the use of PWHT using the AISI 8630M steel are a consequence of the difficulties and limitations already presented in this paper for that steel (elevated carbon content and hardenability and high tendency to banding). However, that greater level of hardness, besides not being a very elevated difference, cannot necessarily be related to a higher brittleness in the HAZ of these joints.

As mentioned earlier, the joints buttered using the parameters that met the selected criteria presented an elevated degree of grain refinement in the HAZ, while, the samples buttered with the conventional technique presented HAZ with extremely coarse microstructure.

The elevated refinement in the samples that met the selected criteria may be more significant than the hardness levels found and can elevate the toughness of these joints in relation to the ones buttered using the conventional technique.

Figure 11a shows the microhardness profiles found along the HAZ of some of the studied joints.

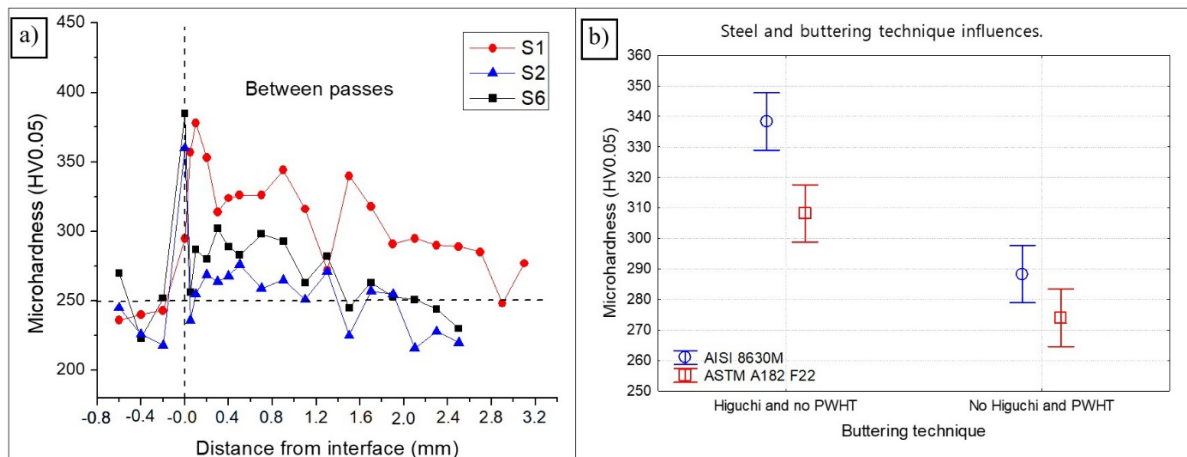


**Figure 11.** a) Microhardness profiles between passes of the welded joints. b) Analysis of variance of the steel and buttering technique used.

The results shown in Figure 11a confirm the hardness results presented previously. However, in the microhardness analysis, aspects like banding become much more evident (especially for the AISI 8630M steel joints). Besides, the microhardness tests show that the more critical points in the HAZ are in the regions between passes, this result can be associated to a greater difficulty to efficiently superimpose the heat cycles in these regions.

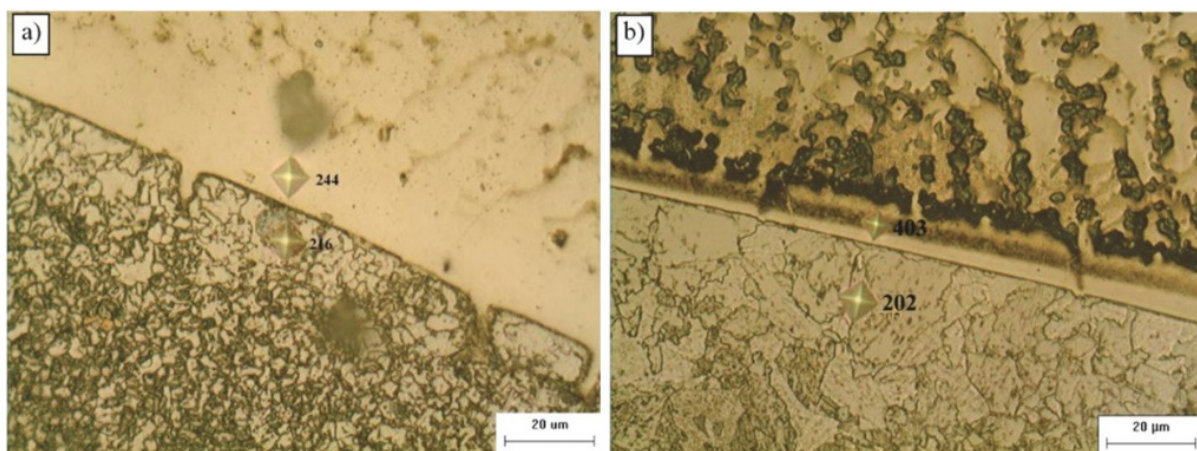
Figure 11a, for example, clearly demonstrates the lower hardness values in the HAZ of the joint buttered with the condition approved by the decision diagrams with PWHT (S2) in comparison to the joint also submitted to PWHT but buttered with a condition not approved (S6).

Figure 11b presents an analysis of variance of the effect of the steel and buttering technique used on the microhardness found in the HAZ (up to 1 mm from the dissimilar interface) of the analyzed samples.

The results shown in Figure 11b follow in the same direction as the hardness results in Figure 10, with lower hardness associated to the ASTM A182 F22 steel and to the use of PWHT. However, the microhardness tests presented higher values than the hardness tests and, besides that, the difference associated to the use of DL-CDT without PWHT and the conventional technique with PWHT was also higher. This result is associated mainly to the microscopic nature of the microhardness tests where more localized analyses were performed.

An important result that was not identified by means of the hardness tests is the increase of microhardness in the buttering interface with the steel samples submitted to PWHT. Figure 11 shows that the profiles associated to the joints where PWHT was used presented microhardness levels on the interface region (position 0,0 on the x axis of the graphs) higher than the profiles associated to the joints buttered without PWHT.

This result was found only in the joints buttered with a nickel alloy because of the dissimilar interface formed between that alloy and the steels used and is attributed to the diffusion of the carbon to that region during PWHT [5,7,24]. Figure 12 shows an example of the interface where there was an increase in the microhardness due to the use of PWHT.



**Figure 12.** Microhardness measured on the interface of AISI 8630M steel buttered a) without PWHT and b) with PWHT.

Such results may lead to the need for greater caution when using the NACE MR0175 norm, with respect to the hardness criterion. As shown in Figure 9b, the AISI 8630M joint submitted to PWHT, presented hardness values in the HAZ lower than the

250 HV10 limited by the NACE MR0175 norm which, according to the same, minimizes the possibility of problems with hydrogen fragilization in such a joint. However, according to Figure 11a, even after performing PWHT, the interface region presented values of microhardness close to 400 HV0.05 which may suggest a possible fragilization in that region.

These regions of elevated hardness may be found in the interface with different morphologies and extensions. The development of these regions is attributed [25-32] to the formation of a laminar flow zone near the weld pool dissimilar interface. These regions are critical because they have an intermediate chemical composition to steel base metal and nickel filler metal alloy, which with the welding thermal cycle, can lead to the formation of fragile zones, even after PWHT.

#### 4. Conclusion

This paper has shown that the combination of both hardness and microstructure criteria in DL-CDT with the LPTS decision diagrams allows the relationships between the buttering parameters for the AISI 8630M and ASTM A182 F22 steels, without the need for PWHT to be determined. The elimination of PWHT, which is main contribution of this method, resulted in joints with refined HAZ and maximum hardnesses of 325 HV10 and 250HV10, respectively. These levels are in line with those of joints manufactured by the conventional method that includes the use of PWHT.

#### Acknowledgements

The authors of this paper are grateful to LPTS – UFC for all the infrastructure made available for the completion of this paper and to CAPES, CENPES/PETROBRAS and FINEP for the financial support.

#### References

- [1] Silva A, Costa EC, Almeida JG, Maciel TM, Cavalcante DGL, Passos TA. Effect of hydrogen on the mechanical properties of ASTM A182 F22 and ASTM A36 steels welded joint using inconel 625 as filler and buttering metal. *Materials Research*. 2022;25:1-15. <http://dx.doi.org/10.1590/1980-5373-mr-2021-0339>.
- [2] Frei J, Alexandrov B, Rethmeier M. Low heat input gas metal arc welding for dissimilar metal weld overlays part II: the transition zone. *Welding in the World*. 2018;62(2):317-324. <http://dx.doi.org/10.1007/s40194-017-0539-5>.
- [3] Kulkarni A, Dwivedi D, Vasudevan M. Dissimilar metal welding of P91 steel-AISI 316L SS with Incoloy 800 and Inconel 600 interlayers by using activated TIG welding process and its effect on the microstructure and mechanical properties. *Journal of Materials Processing Technology*. 2019;274:116280. <http://dx.doi.org/10.1016/j.jmatprotec.2019.116280>.
- [4] NACE International. NACE MR175: Petroleum and natural gas industries - Materials for use in H2S-containing environments in oil and gas production. Part 1: General principles for selection of cracking-resistant materials. Houston: NACE; 2015.
- [5] Fenske JA, Robertson IM, Ayer R, Hukle M, Lillig D, Newbury B. Microstructure and hydrogen-induced failure mechanisms in Fe and Ni alloy weldments. *Metallurgical and Materials Transactions A, Physical Metallurgy and Materials Science*. 2012;43(9):3011-3022. <http://dx.doi.org/10.1007/s11661-012-1129-1>.
- [6] Fenske JA. Microstructure and hydrogen induced failure mechanisms in iron-nickel weldments [doctor thesis]. Illinois: University of Illinois; 2010.
- [7] Olden V, Olden V, Kvaale PE, Simensen PA, Aaldstedt S, Solberg JK. The effect of PWHT on the material properties and microstructure in Inconel 625 and Inconel 725 buttered joints. In: American Society of Mechanical Engineers. The 22nd International Conference on Offshore Mechanics & Arctic Engineering. Cancun, Mexico. New York: American Society of Mechanical Engineers; 2003.
- [8] Miranda HC. Aplicação da dupla camada na soldagem de aços ASTM A516 Gr. 70: relatório técnico. Fortaleza: Universidade Federal do Ceará; 2009.
- [9] Higuchi M, Sakamoto H, Tanioka S. A study on weld repair through half bead method. *IHI Engineering Review*. 1980;13(2):14-19.
- [10] Nogoya International Training Center. Precaution against failure of heat treatment. Japan: Japan International Cooperation Agency; 1974.
- [11] Welding Technology Institute of Australia. Temper bead welding. Australia: WTIA; 2006.
- [12] Lundin CD, Wang Y, Batten G. Literature survey of half-bead, temperbead, controlled deposition techniques for improvement of fabrication and service performance of Cr-Mo steels. New York: WRC - Welding Research Council; 2005.
- [13] Silva CC, Albuquerque VHC, Moura CRO, Aguiar WM, Farias JP. Evaluation of AISI 4140 steel repair without post-weld heat treatment. *Journal of Materials Engineering and Performance*. 2009;18(3):324-331. <http://dx.doi.org/10.1007/s11665-008-9294-5>.
- [14] Pinheiro PHM. Estudo da soldagem MIG/MAG aplicada a reparo dos aços Cr-Mo e Cr-Mo-V utilizando a técnica de deposição controlada com dupla camada. [tese de doutorado]. Fortaleza: Centro de Tecnologia, Universidade Federal do Ceará; 2017.
- [15] Cavalcante NE, Andrade TC, Pinheiro PHM, Miranda HC, Motta MF, Aguiar WM. Estudo de procedimentos de soldagem MIG/MAG para aplicação de revestimentos de liga de níquel inconel 625 em aço estrutural ASTM A387 Gr.11. *Soldagem e Inspeção*. 2016;21(1):70-82. <http://dx.doi.org/10.1590/0104-9224/SI2101.07>.



- [16] Capdevila C, Garcia-Junceda A, Capdevila C, Andres CG. Evolution of microstructural banding during the manufacturing process of dual phase steels. *Materials Transactions*. 2006;2276:2269-2276.
- [17] Grange RA. Effect of microstructural banding in steel. *Metallurgical Transactions*. 1971;2(2):417-426. <http://dx.doi.org/10.1007/BF02663328>.
- [18] Krawczyk J, Pawłowski B, Bała P. Banded microstructure in forged 18CrNiMo7-6 Steel. *Metallurgy and Foundry Engineering*. 2013;35(1):45-53. <http://dx.doi.org/10.7494/mafe.2009.35.1.45>.
- [19] Verhoeven J. A review of microsegregation induced banding phenomena in steels. *Journal of Materials Engineering and Performance*. 2000;9(3):286-296. <http://dx.doi.org/10.1361/105994900770345935>.
- [20] Silva C, Albuquerque VHC, Moura CRO, Aguiar WM, Farias JP. Evaluation of AISI 4140 steel repair without post-weld heat treatment. *Journal of Materials Engineering and Performance*. 2009;18(3):324-331. <http://dx.doi.org/10.1007/s11665-008-9294-5>.
- [21] Albuquerque VHCD, Silva CC, Moura CRO, Aguiar WM, Farias JP. Effect of nonmetallic inclusion and banding on the success of the two-layer temper bead welding technique. *Materials & Design*. 2009;30(4):1068-1074. <http://dx.doi.org/10.1016/j.matdes.2008.06.056>.
- [22] Magalhães SG. Avaliação do revestimento a base de liga de níquel em aço estrutural empregando o metal de adição ERNiCrMo-3 através da soldagem MIG/MAG [dissertação de mestrado]. Fortaleza: Universidade Federal do Ceará; 2008.
- [23] Aguiar WM. Revestimento por soldagem MIG/MAG empregando ligas de níquel para aplicações em componentes do setor Petróleo e Gás Natural [tese de doutorado]. Fortaleza: Departamento de Engenharia Metalúrgica e de Materiais, Universidade Federal do Ceará; 2010.
- [24] Alexandrov BT, Lippold JC, Sowards JW, Hope AT, Saltzmann DR. Fusion boundary microstructure evolution associated with embrittlement of Ni-base alloy overlays applied to carbon steel. *Welding in the World*. 2013;57(1):39-53. <http://dx.doi.org/10.1007/s40194-012-0007-1>.
- [25] Baeslack WA, Lippold JC, Savage WF. Unmixed zone formation in austenitic stainless steel weldments. *Welding Journal*. 1979;58(6):169-176.
- [26] Beaugrand VCM, Smith LS, Gittos MF. Subsea dissimilar joints: failure mechanisms and opportunities for mitigation. In: *NACE Corrosion 2009*. Atlanta, Georgia, USA: NACE; 2009.
- [27] Doody T. Intermediate mixed zones in dissimilar metal welds for sour service. *Welding Journal*. 1992;71:55-60.
- [28] Kejelin NZ, Buschinelli AJA, Pope AM. Influence of welding parameters on the formation of partially diluted zones of dissimilar metal welds. *Soldagem e Inspeção*. 2007;12(3):195-203.
- [29] Omar AA. Effects of welding parameters on hard zone formation at dissimilar metal welds. *Welding Journal*. 1998;87(2):86-93.
- [30] Rowe MD, Nelson TW, Lippold JC. Hydrogen-induced cracking along the fusion boundary of dissimilar metals welds. *Welding Journal*. 1999;78(2):31-37.
- [31] Silva CC, Miranda HC, Motta MF, Farias JP. Influence of welding in operational conditions on the partial mixed zone formation in Ni-Based dissimilar weld overlay. In: *Trends in Welding Research: Proceedings of the 9th International Conference*. Ohio: ASM international; 2013.
- [32] Silva CC, Miranda HC, Farias JP, Abreu HFG. Chemistry and crystallographic evaluation of ni-based alloys and steels dissimilar interface. In: *Trends in Welding Research: Proceedings of the 9th International Conference*. Chicago, Illinois, USA Ohio: ASM international; 2013.